Check for updates

Pb$_6$Ba$_3$Si$_2$S$_8$I$_{10}$: a new thiohalide with a quasi-two-dimensional structure and wide band gap†

Wang Zhao, [a,b] Jiazheng Zhou, [a] Linan Wang, [a,b] Wenqi Jin, [a,b] Yingying Kong, [a] Yu Chu (ID) *[a,b] and Junjie Li (ID) *[a,b]

Pb-based chalcogenides display abundant structural diversity and distinguished properties. Based on a mixed anion and dimensional reduction combined strategy, a wide band gap Pb-based thiohalide, Pb$_6$Ba$_3$Si$_2$S$_8$I$_{10}$, has been rationally designed and synthesized experimentally by the flux method. The compound crystallizes in the $R\bar{3}c$ space group with cell parameters a = 9.7925(2) Å, b = 9.7925(2) Å, and c = 70.628(3) Å and is composed of [SiS$_4$] tetrahedra and unprecedented [PbI$_5$S$_2$] polyhedral units, resulting in a unique quasi-two-dimensional structure, which enriches the chemical and structural diversity of Pb-based thiohalides. The experimental band gap of Pb$_6$Ba$_3$Si$_2$S$_8$I$_{10}$ was determined to be 2.80 eV. Based on statistical analyses and to the best of our knowledge, it is the largest experimental optical band gap among the known Pb-based thiohalides. The results demonstrate the feasibility of using highly electropositive Ba atoms to regulate the dimensions of the structural framework of thiohalides and give new insights into the structure and property modifications of thiohalides by the mixed anion and dimensional reduction combined strategy.

Introduction

The development of functional materials and structural chemistry is highly dependent on the discovery of new compounds with distinctive crystal structures and physicochemical properties.[1–8] Introducing cations with stereochemically active lone-pair electrons, such as Pb^{2+}, Sn^{2+}, Bi^{3+}, Sb^{3+}, and As^{3+}, has been demonstrated as an effective strategy to enhance the optical anisotropy of optoelectronic functional materials.[9–13] Among them, Pb^{2+}-containing compounds with stereochemically active lone-pair electrons are conducive to inducing a significant second-harmonic generation (SHG) response, but they usually exhibit an adverse effect on the band gap, such as PbGa$_2$GeSe$_6$ (1.96 eV, 5 × AgGaS$_2$ (AGS)), Pb$_{0.65}$Mn$_{2.85}$Ga$_3$S$_8$ (1.68 eV, 1.5 × AGS), Pb$_{0.72}$Mn$_{2.84}$Ga$_{2.95}$Se$_8$ (1.65 eV, 4.4 × AGS), Pb$_4$Ga$_4$GeS$_{12}$ (2.18 eV, 2 × AGS), and PbGa$_4$Se$_7$ (2.1 eV, 3.3 × AGS).[14–20] As a critical parameter of optoelectronic functional materials, a wide band gap can effectively suppress two-photon/multi-photon absorption in IR nonlinear optical materials. For instance, a material with a band gap wider than 2.33 eV can only be effectively pumped by mature 1064 nm laser sources in the absence of two-photon absorption and free carrier absorption. Moreover, a larger band gap is advantageous for the compound to achieve a higher laser-induced damage threshold.[21–27] Thus, it is important to overcome the drawback of the narrow band gap in Pb-based chalcogenides.

Recently, introducing highly electronegative halogens has been proved to be a feasible strategy to increase the band gap of Pb-based chalcogenides,[28–37] and a series of Pb-based salt-inclusion chalcogenides have been developed, such as [K$_2$PbI][Ga$_7$S$_{12}$] (2.41 eV), [K$_2$PbBr][Ga$_7$S$_{12}$] (2.49 eV), [K$_2$PbCl][Ga$_7$S$_{12}$] (2.54 eV), [Na$_2$PbI][Ga$_7$S$_{12}$] (2.53 eV), Pb$_3$S$_3$Cl$_2$ (2.02 eV), Pb$_3$SBrI$_3$ (2.16 eV), Pb$_2$SbS$_2$I$_3$ (2.19 eV), Pb$_4$SeBr$_6$ (2.62 eV), Pb$_{3.5}$GeS$_4$Br$_3$ (2.6 eV), *etc*.[38–50] In addition, reducing the dimensions of the crystal structure using highly electropositive/negative elements is also helpful in increasing the optical band gap of inorganic compounds, and this has been demonstrated in many systems, such as sulfides,[51,52] selenides,[53] tellurides and carbonates.[54]

In this work, based on a mixed anion and dimensional reduction (introducing highly electropositive Ba atoms) combined strategy, a new Pb-based thiohalide Pb$_6$Ba$_3$Si$_2$S$_8$I$_{10}$ with unprecedented [PbI$_5$S$_2$] octahedra has been rationally designed and synthesized by the flux method. The compound crystallizes in the centrosymmetric $R\bar{3}c$ space group and shows a quite large cell parameter c = 70.628(3) Å (due to the presence of six distinct filling modes of Ba and I atoms in the layers),

[a]Research Center for Crystal Materials; CAS Key Laboratory of Functional Materials and Devices for Special Environments, Xinjiang Technical Institute of Physics & Chemistry, CAS, Urumqi 830011, China. E-mail: lijunjie@ms.xjb.ac.cn, chuy@ms.xjb.ac.cn

[b]Center of Materials Science and Optoelectronics Engineering, University of Chinese Academy of Sciences, Beijing 100049, China

resulting in a quasi-two-dimensional (quasi-2D) crystal structure composed of tetrahedral $[SiS_4]$ and polyhedral $[PbI_5S_2]$ units. The formed quasi-2D structure is different from the three-dimensional (3D) frameworks in most of the Pb-based thiohalides. Moreover, due to the introduction of alkaline-earth metal (AEM) Ba and I atoms into the compound simultaneously, a relatively wide band gap (among the thiohalides) of 2.80 eV in the title compound is achieved.

Experimental section

Reagents

BaS (Aladdin, 99.7%), Pb (Aladdin, 99.9%), PbI_2 (Aladdin, 99.99%), Si (Aladdin, 99.99%), and S (Sinopharm, 99.9%) were purchased commercially and used as the starting materials without further purification.

Synthesis

The single crystal of the title compound for structural determination (Table 1) was grown by the flux method[55,56] with $PbCl_2$ as the flux in a sealed quartz tube at ~950 °C. The details for the crystal growth are shown as follows: (1) the mixtures of BaS (0.094 g), Pb (0.038 g), Pbl_2 (0.427 g), Si (0.030 g) and S (0.010 g) were ground and loaded into a graphite crucible with an inner diameter of 7 mm; (2) the crucible was transferred into a 10 mm (inner diameter) quartz tube, and it was further sealed with a methane-oxygen flame under a high vacuum of 10^{-3} Pa; and (3) the sealed tube was placed into a computer-controlled furnace and then heated to 950 °C for 24 h and kept at this temperature for 48 h, cooled to 650 K at a rate of 1 °C h^{-1}, and then cooled to room temperature naturally. The pure phase powder samples were prepared in sealed quartz

tubes with the starting materials of $BaS : Pb : PbI_2 : Si : S = 3 : 1 : 5 : 2 : 5$ (molar ratio). The temperature program for the chemical synthesis involved quickly heating up to 950 °C and maintaining that temperature for 48 h, and then cooling to room temperature rapidly. Finally, the polycrystalline powder samples of $Pb_6Ba_3Si_2S_8I_{10}$ were harvested at the bottom with some impurities on the top of the tubes.

Structural determination

A yellow and transparent $Pb_6Ba_3Si_2S_8I_{10}$ single crystal with a size of $0.15 \times 0.05 \times 0.04$ mm^3 was selected for the structural characterization. The data were collected on a Bruker Smart APEX III. The crystal structure was solved by direct methods and then refined by full-matrix least squares on F^2 with the SHELXTL-14 program.[57,58] The PLATON program was used to check the possible missing symmetry elements and no higher symmetry was suggested in the structure.[59] The crystallographic data are available at CCDC 2369466† in CIF format.

Powder X-ray diffraction (PXRD)

PXRD data of $Pb_6Ba_3Si_2S_8I_{10}$ were collected on a Bruker D2 PHASER X-ray diffractometer equipped with Cu Kα radiation (λ = 1.54056 Å) at room temperature and the diffraction patterns were taken from 10° to 70° (2θ).[60,61] Then, powder Rietveld refinement was performed using GSAS software.

Energy dispersive X-ray spectroscopy (EDS)

The EDS spectrum of the title compound was recorded on a field emission scanning electron microscope (FE-SEM, JEOL JSM-7610F Plus, Japan) with an energy dispersive X-ray spectrometer (Oxford, X-Max 50) at room temperature. It was operated at 5 kV.

UV-vis-NIR diffuse reflectance and infrared (IR) spectra

The UV-vis-NIR diffuse reflectance spectrum of $Pb_6Ba_3Si_2S_8I_{10}$ was characterized on a Shimadzu SolidSpec-3700DUV spectrophotometer at room temperature within a wavelength range from 180 to 2600 nm. The reflectance spectrum was converted to pseudo-absorption data based on the Kubelka–Munk function: $F(R) = (1 - R)^2/2R = K/S$ (R = reflectance; K = absorption; and S = scattering).[62] Before recording the IR spectrum, the polycrystalline $Pb_6Ba_3Si_2S_8I_{10}$ powder sample was made into a pellet with KBr powder. The IR spectrum of the compound was recorded on a Shimadzu IR Affinity-1 Fourier transform infrared spectrometer within a range of 4000–400 cm^{-1}.

Refractive index difference (RID)

The RID of the $Pb_6Ba_3Si_2S_8I_{10}$ single crystal was tested on a polarizing microscope equipped (ZEISS Axio Scope. 5 pol) with a Berek compensator. The wavelength of the used light source was 546 nm. The difference in the optical path (D) for one direction was determined according to the interference color with the maximum value of the crystal under polarized light.[63] The RID can be calculated from the following equation: $D = |N_2 - N_1| \times T = \Delta n \times T$, where Δn represents the difference in the refractive index and T is the thickness of the crystal.[64]

Table 1 Crystallographic data and structure refinements for $Pb_6Ba_3Si_2S_8I_{10}$

Empirical formula	$Pb_6Ba_3Si_2S_8I_{10}$
Formula weight	3236.76
Temperature	298.15 K
Crystal system, space group	Trigonal, $R\bar{3}c$
Unit cell dimensions	$a = 9.7925(2)$ Å
	$b = 9.7925(2)$ Å
	$c = 70.628(3)$ Å
Volume	5865.4(3) Å^3
Z, calculated density	6, 5.498 g cm^{-3}
Absorption coefficient	37.085 mm^{-1}
$F(000)$	8076
Data/restraints/parameters	1870/0/47
Index ranges	$-13 \leq h \leq 12$, $-8 \leq k \leq 9$, $-89 \leq l \leq 98$
Completeness	99.0%
Independent reflections	1870 [$R_{int} = 0.0465$, $R_{sigma} = 0.0403$]
GOF on F^2	1.074
2θ range for data collection	4.94° to 60.068°
Reflections collected	8103
Final R indices [$F_o^2 > 2\sigma(F_o^2)$][a]	$R_1 = 0.0434$, w$R_2 = 0.0869$
R indices (all data)[a]	$R_1 = 0.0540$, w$R_2 = 0.0911$
Largest diff. peaks and holes	2.11/−2.19 e Å^{-3}

[a] $R_1 = \sum||F_o| - |F_c||/\sum|F_o|$ and w$R_2 = [\sum w(F_o^2 - F_c^2)^2/\sum wF_o^4]^{1/2}$ for $F_o^2 > 2\sigma(F_o^2)$.

Computational methods

The first-principles calculations were performed by the plane wave pseudopotential method implemented in the CASTEP package.[65,66] The generalized gradient approximation (GGA) and Perdew–Burke–Ernzerhof (PBE) functional were adopted for the calculations, and the norm-conserving pseudopotentials (NCPs) were used to calculate the electronic structure and optical properties.[67] The cutoff energy was set to 820 eV. In order to model the effective interactions between valence electrons and the atom cores in $Pb_6Ba_3Si_2S_8I_{10}$, the valence electrons were set as $Ba-5s^25p^66s^2$, $Pb-5s^25p^65d^{10}6s^26p^2$, $Si-3s^23p^2$, $S-3s^23p^4$, and $I-5s^25p^5$. The Monkhorst–Pack k-point grid was set to $3 \times 3 \times 3$ in the Brillouin zone (BZ). The residual calculation parameters and convergent criteria were set to the default values in the CASTEP package.

Results and discussion

The results of single crystal XRD show that $Pb_6Ba_3Si_2S_8I_{10}$ crystallizes in the trigonal $R\bar{3}c$ space group with cell parameters a = 9.7925(2) Å, b = 9.7925(2) Å, c = 70.628(3) Å, V = 5865.36(35) Å^3 and Z = 6. The crystallographic data and structure refinement information for $Pb_6Ba_3Si_2S_8I_{10}$ are provided in Table 1, and the atomic coordinates, bond distances, angles, and isotropic displacement parameters are given in Tables S1 and S2.† The calculated bond valence sums (Pb^{2+}: 1.83, Ba^{2+}: 2.31, Si^{4+}: 3.94, S^{2-}: 2.12–2.15, and I^-: 0.79–1.55 for $Pb_6Ba_3Si_2S_8I_{10}$) and small global instability indices GII = 0.178 (Table S1†) verify the reasonability of the crystal structure. The results of EDS spectroscopy and mapping (Fig. S1†) confirm the presence of Pb, Ba, Si, S, and I in the structure.

In the asymmetric unit of $Pb_6Ba_3Si_2S_8I_{10}$, there is one crystallographically independent Pb atom, one Ba atom, one Si atom, two S atoms and four I atoms. The Si atoms are coordinated with four S atoms to form $[SiS_4]$ tetrahedral units with the bond lengths of $d_{(Si-S)}$ = 2.112–2.152 Å (Fig. 1a). The Pb atoms are coordinated with two S and six I atoms to build $[PbI_5S_2]$ polyhedral units (Fig. 1b) with $d_{(Pb-I)}$ = 3.344–3.548 Å and $d_{(Pb-S)}$ = 2.821–2.883 Å. The formed $[PbI_5S_2]$ mixed anionic unit is totally different from the formed $[PbS_5Cl_2]$ in $Pb_5Sn_3S_{10}Cl_2$,[47] $[PbS_4Br_4]$, $[PbS_5Br_3]$, $[PbS_6Br_2]$ in $Pb_4S_3Br_2$,[41] $[PbSI_4]$ in Pb_3SBrI_3,[46] and $[PbS_3I_5]$ and $[PbSBrI_5]$ in Pb_3SBrI_3.[45] Based on statistical investigations using the Inorganic Crystal Structure Database (ICSD-5.2.0, the latest release of ICSD-2024/04/10) and to the best of our knowledge, $[PbI_5S_2]$ is for the first time observed in Pb-based thiohalide compounds. Furthermore, the six $[PbI_5S_2]$ octahedra are further interconnected with each other by edge-sharing to construct a $[Pb_6I_{13}S_{12}]$ polymer (Fig. 1c). The formed $[Pb_6I_{13}S_{12}]$ polymers are linked by tetrahedral $[SiS_4]$ units in a vertex-sharing way to produce 2D Pb–Si–S–I layers (Fig. 1d). The Ba and partial I atoms are located in the gaps of 2D Pb–Si–S–I layers to balance the valence states, resulting in the final quasi-2D structure of the title compound.

Compared to the 3D Pb–S–Cl and Pb–S–Br frameworks in $Pb_5Sn_3S_{10}Cl_2$[47] and $Pb_4S_3Br_2$,[48] respectively, the Pb–S–I framework is reduced to a 2D structure in $Pb_6Ba_3Si_2S_8I_{10}$, due to the introduction of highly electropositive Ba atoms with a high atomic proportion. In addition, from the perspective of Ba–I layers, Ba atoms exhibit three distinct arrangements, referred to as A, B, and C in Fig. S2.† The arrangements give rise to A', B', and C' through a combination of secondary screw axes and glide symmetry operations along the c-direction, preventing the Ba atom layer from repeating within the unit cell via translational operations. The interleaved arrangements of Ba and I atoms ultimately result in six unique Ba–I configurations along the c-axis. Hence, due to the presence of six distinct
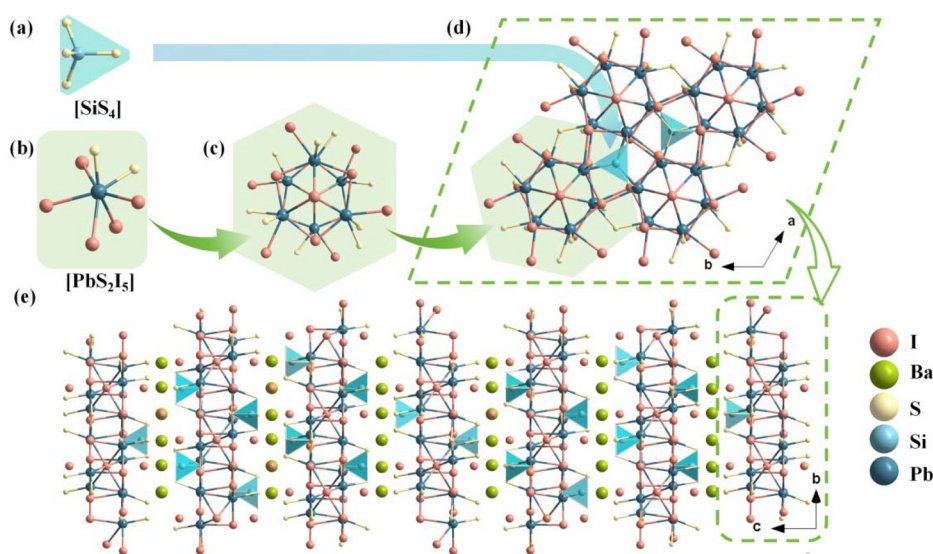

Fig. 1 Crystal structure of $Pb_6Ba_3Si_2S_8I_{10}$. (a and b) The coordination mode of Si (a) and Pb atoms (b); (c) the formed $[Pb_6I_{13}S_{12}]$ group; (d) the resultant 2D Pb–Si–S–I layer; and (e) the quasi-2D structure of $Pb_6Ba_3Si_2S_8I_{10}$.

filling modes of Ba and I atoms between the inter-layers of 2D Pb–Si–S–I, a large cell parameter $c = 70.628(3)$ Å is observed in $Pb_6Ba_3Si_2S_8I_{10}$. To confirm the chemical bonding and optical absorption regions, the IR spectrum of $Pb_6Ba_3Si_2S_8I_{10}$ was recorded on a Shimadzu IR Affinity-1 Fourier transform infrared spectrometer, and it shows three strong absorption peaks at 501 cm^{-1}, 534 cm^{-1} and 1084 cm^{-1}, which can be attributed to the characteristic vibrations of Si–S bonding.[68] Besides, the absorption peak at 785 cm^{-1} originates from the in-plane bending vibration of carbon dioxide (Fig. S3†).[69]

To elucidate the influence of highly electropositive cations on the structural dimension in Pb-based thiohalides, we extended the investigation to the all-known alkali metal (AM)- and/or AEM-containing Pb-based thiohalides in the ICSD, and 16 Pb-based thiohalides without C, H, O, and N elements are summarized in Table S3.† It can be seen that, except $Pb_6Ba_3Si_2S_8I_{10}$ with a quasi-2D structure, all the known compounds including $[Na_2PbI][Ga_7S_{12}]$, $[K_2PbI][Ga_7S_{12}]$, $[K_2PbBr][Ga_7S_{12}]$, and $[K_2PbCl][Ga_7S_{12}]$ show 3D frameworks. Previous investigations indicate that the atomic ratio between electropositive AM/AEM cations and other central atoms capable of forming polyhedral units plays an important role in determining the dimensions of polyhedron-based frameworks.[70] Based on statistical investigations, when the A/(Pb + M) ratio (where A represents highly electropositive AM or AEM atoms, while M denotes other central atoms capable of forming polyhedral units) is smaller than about 0.3, the compounds show 3D frameworks (Fig. 2a). Taking $[Na_2PbI][Ga_7S_{12}]$ as an example (Fig. 2c, where $Pb_6Ba_3Si_2S_8I_{10}$ is used as a reference in Fig. 2b), the Na/(Pb + Ga) atomic ratio is 0.25, smaller than the Ba/(Pb + Si) ratio of 0.375 in $Pb_6Ba_3Si_2S_8I_{10}$, resulting in a 3D pore-like structure in $[Na_2PbI][Ga_7S_{12}]$, and the Na

atoms are placed in the pores, different from the interlayered Ba atoms in $Pb_6Ba_3Si_2S_8I_{10}$ (Fig. 2b). The results highlight that the proportion of highly electropositive cations affects the crystal structures in thiohalides.

To detect the optical properties, the pure phase polycrystalline powder samples of the title compound were synthesized and characterized. As shown in Fig. 3a, the PXRD pattern of $Pb_6Ba_3Si_2S_8I_{10}$ matches well the theoretical result derived from the CIF file using Mercury. Moreover, to assess the purity of the powder samples, the results of powder Rietveld refinement ($R_{WP} = 4.00\%$ and $R_P = 2.98\%$) have been analysed, which indicate high purity for the obtained polycrystalline samples and confirm the results of single crystal XRD. In addition, to check the thermal stability, XRD characterization before and after melting has been carried out, as shown in Fig. S5.† The results imply that $Pb_6Ba_3Si_2S_8I_{10}$ could be a congruently melting compound, which is favorable for the growth of large-sized single crystals. To detect the experimental optical band gap, the UV-vis-NIR diffuse reflectance spectrum of the title compound was recorded by using the pure phase polycrystalline powder samples. Moreover, based on the $[(k\nu F(R))]^{1/2}$ spectrum (Fig. S6†), the band gap of $Pb_6Ba_3Si_2S_8I_{10}$ was determined to be 2.13 eV, while it was 2.80 eV based on the $[(k\nu F(R))]^2$ spectrum (Fig. 3b). The latter shows good agreement with the color of $Pb_6Ba_3Si_2S_8I_{10}$ (yellow). It is worth noting that the value is larger than those of most of the Pb-based thiohalides, such as $Pb_5Sn_3Se_{10}Cl_2$ (1.44 eV), $Pb_5Sn_3S_{10}Cl_2$ (1.72 eV), $Pb_5S_2I_6$ (1.73 eV), $Pb_4S_3I_2$ (1.76 eV), $Pb_4S_3Br_2$ (1.91 eV), $[K_2PbI][Ga_7S_{12}]$ (2.41 eV), $[K_2PbBr][Ga_7S_{12}]$ (2.49 eV), $[K_2PbCl][Ga_7S_{12}]$ (2.54 eV), $[Na_2PbI][Ga_7S_{12}]$ (2.53 eV), $Pb_3S_3Cl_2$ (2.02 eV), Pb_3SBrI_3 (2.16 eV), $Pb_2SbS_2I_3$ (2.19 eV), Pb_4SeBr_6 (2.62 eV), and $Pb_{3.5}GeS_4Br_3$
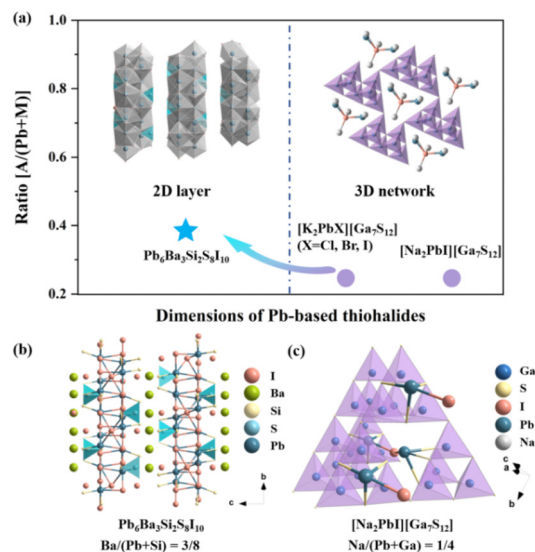
Fig. 2 (a) Relationship between the A/(Pb + M) ratio (A = Na, K, and Ba; M = Ga and Si) and the dimensions of Pb-based thiohalides; structural comparison between quasi-2D $Pb_6Ba_3Si_2S_8I_{10}$ (b) and 3D $[Na_2PbI][Ga_7S_{12}]$ (c).

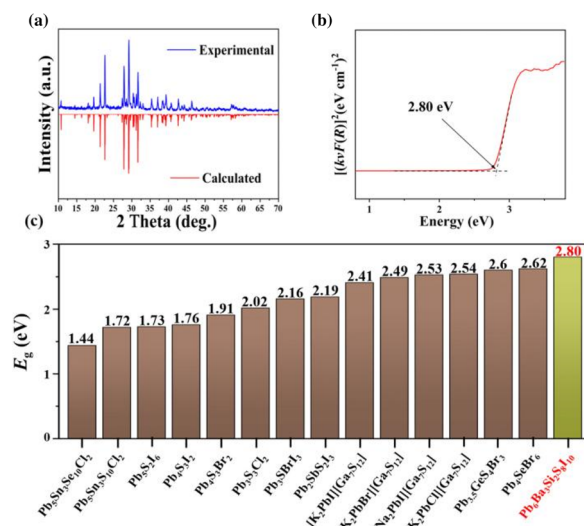**Fig. 3** (a) Experimental and theoretical XRD patterns; (b) diffuse reflectance spectrum of $Pb_6Ba_3Si_2S_8I_{10}$ plotted as $[(k\nu F(R))]^2$ (direct band gap), where $F(R)$ is the Kubelka–Munk function. Dotted lines show the fit used to extract the band gap; (c) the statistical investigations on the band gaps of typical Pb-based thiohalides (brown: 3D structured compounds and green: quasi-2D structured compounds).
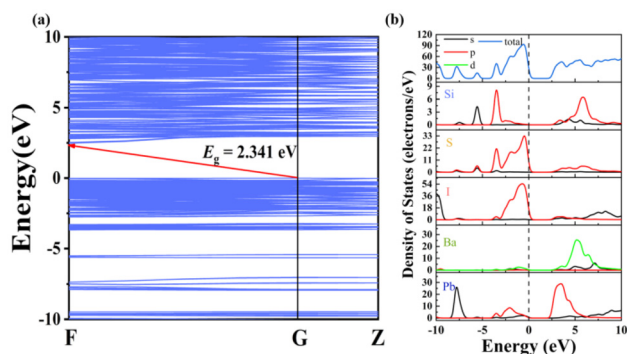
Fig. 4 (a) The band structure of $Pb_6Ba_3Si_2S_8I_{10}$ and (b) the total and partial densities of states of $Pb_6Ba_3Si_2S_8I_{10}$.

(2.6 eV) (Fig. 3c).[38–50] The reason for the relatively wide band gap in $Pb_6Ba_3Si_2S_8I_{10}$ could be related to the low-dimensional quasi-2D structure, similar to the cases of $A^{II}HgM^{IV}S_4$ (A^{II} = Sr and Ba; M^{IV} = Si and Ge) (2.94–3.06 eV),[71] $PbFIO_3$ (3.87 eV),[72] and $AEGe_2O_4Se$ (AE = Sr and Ba) (3.57 and 3.81 eV).[73] Moreover, the RID of $Pb_6Ba_3Si_2S_8I_{10}$ was determined to be 0.006 at 546 nm (Fig. S7†).

To detect the origin of optical properties in $Pb_6Ba_3Si_2S_8I_{10}$, density functional theory (DFT) calculations were performed. The band structure indicates that $Pb_6Ba_3Si_2S_8I_{10}$ is an indirect band gap semiconductor with a calculated GGA band gap of 2.341 eV (Fig. 4a), smaller than the experimental value of 2.80 eV, because of the discontinuity of the exchange–correlation energy functional.[74] From the density of states (DOS) and partial DOS (PDOS) diagram in Fig. 4b, it can be seen that the top of the valence band (VB) is mainly derived from the S-3p and I-5p orbitals, while the bottom of the conduction band (CB) is occupied by the Pb-6p orbital (Fig. 4b). It indicates that the optical band gap in the title compound is mainly determined by the rare $[PbI_5S_2]$ units, indicating the positive contribution of the mixed anions.[30]

Conclusions

In summary, a new Pb-based thiohalide $Pb_6Ba_3Si_2S_8I_{10}$ with unprecedented $[PbI_5S_2]$ mixed anionic units has been designed by a mixed anion and dimensional reduction combined strategy and synthesized experimentally. The crystal structure of the compound was determined by single crystal XRD, and it shows a quasi-2D structure that is composed of polyhedral $[PbI_5S_2]$ and tetrahedral $[SiS_4]$ units. More importantly, the introduction of highly electropositive Ba atoms with a high atomic proportion reduces the structural dimension, resulting in a relatively wide band gap of 2.80 eV in $Pb_6Ba_3Si_2S_8I_{10}$, which is higher than those of known Pb-based thiohalides. DFT calculations indicate that $Pb_6Ba_3Si_2S_8I_{10}$ is an indirect band gap semiconductor and that the band gap mainly originates from the interaction of the S-3p and I-5p orbitals in the unique $[PbI_5S_2]$ mixed-anionic units. Experimental and theore-

tical results imply that introducing mixed anions and highly electropositive cations simultaneously is a feasible strategy to develop wide band gap Pb-based thiohalides.

Data availability

Supporting data for this article are presented in the ESI.† The raw data of this article can be obtained from the corresponding author upon reasonable request.

Conflicts of interest

The authors declare that they have no conflict of interest.

Acknowledgements

References

1 M. Mutailipu, K. R. Poeppelmeier and S. Pan, *Chem. Rev.*, 2021, **121**, 1130–1202.
2 J. Li and F. L. Deepak, *Chem. Rev.*, 2022, **122**, 16911–16982.
3 M. Mutailipu, J. Han, Z. Li, F. Li, J. Li, F. Zhang, X. Long, Z. Yang and S. Pan, *Nat. Photonics*, 2023, **17**, 694–701.
4 Z. Gong, X. Wang, W. Pi, N. Yao, Z. Fang, H. Bao and Q. Wu, *Mater. Today Phys.*, 2024, **43**, 101399.
5 Y.-G. Chen, X. Hu, Y. Guo, S. Zhao, B. Zhang, X. Zhang and X.-M. Zhang, *Chem. Mater.*, 2024, **36**, 4775–4781.
6 X. Fan, *Crit. Rev. Environ. Sci. Technol.*, 2022, **52**, 2227–2269.
7 G. Shi, Y. Wang, F. Zhang, B. Zhang, Z. Yang, X. Hou, S. Pan and K. R. Poeppelmeier, *J. Am. Chem. Soc.*, 2017, **139**, 10645–10648.
8 G. Deokar, N. S. Rajput, J. Li, F. L. Deepak, W. Ou-Yang, N. Reckinger, C. Bittencourt, J.-F. Colomer and M. Jouiad, *Beilstein J. Nanotechnol.*, 2018, **9**, 1686–1694.
9 Z.-X. Zheng, Z.-X. Qiu, C.-H. Xie, Y.-P. Zhang, X.-M. Jiang, B.-W. Liu and G.-C. Guo, *Sci. China Mater.*, 2023, **66**, 2795–2802.
10 L. Wang, Q. Sun and J. Li, *Chin. J. Struct.*, 2023, **42**, 100013.
11 T. K. Bera, J.-H. Song, A. J. Freeman, J. I. Jang, J. B. Ketterson and M. G. Kanatzidis, *Angew. Chem., Int. Ed.*, 2008, **47**, 7828–7832.
12 J. Wang, B. Xiong, H. Wu, H. Yu, Z. Hu, J. Wang and Y. Wu, *Inorg. Chem. Front.*, 2021, **8**, 344–351.
13 M. Yan, H.-G. Xue and S.-P. Guo, *Cryst. Growth Des.*, 2021, **21**, 698–720.

14 Z.-Z. Luo, C.-S. Lin, H.-H. Cui, W.-L. Zhang, H. Zhang, H. Chen, Z.-Z. He and W.-D. Cheng, *Chem. Mater.*, 2015, **27**, 914–922.

15 M. Zhou, X. Jiang, Y. Guo, Z. Lin, J. Yao and Y. Wu, *Inorg. Chem.*, 2017, **56**, 8454–8461.

16 W. Yin, A. K. Iyer, C. Li, X. Lin, J. Yao and A. Mar, *J. Solid State Chem.*, 2016, **241**, 131–136.

17 X. Chen, H. Jo and K. M. Ok, *Angew. Chem., Int. Ed.*, 2020, **59**, 7514–7520.

18 A.-Y. Wang, S.-H. Zhou, M.-Y. Ran, B. Li, X.-T. Wu, H. Lin and Q.-L. Zhu, *Inorg. Chem. Front.*, 2024, **11**, 3744–3754.

19 J.-H. Zhang, S. S. Stoyko, A. J. Craig, P. Grima, J. W. Kotchey, J. I. Jang and J. A. Aitken, *Chem. Mater.*, 2020, **32**, 10045–10054.

20 G. Peng, C. Lin, H. Fan, K. Chen, B. Li, G. Zhang and N. Ye, *Angew. Chem.*, 2021, **133**, 17555–17558.

21 L. Wang, D. Chu, Z. Yang, J. Li and S. Pan, *Chem. Sci.*, 2024, **15**, 6577–6582.

22 H. Qiu, F. Li, C. Jin, Z. Yang, J. Li, S. Pan and M. Mutailipu, *Angew. Chem., Int. Ed.*, 2024, **63**, e202316194.

23 H. Wang, X. Pan, W. Zhao, Y. Chu and J. Li, *Inorg. Chem. Front.*, 2023, **10**, 6253–6261.

24 H. Wang, Y. Chu, X. Pan, Z. Yang, S. Pan and J. Li, *Mater. Today Phys.*, 2023, **38**, 101243.

25 P. Wang, Y. Chu, A. Tudi, C. Xie, Z. Yang, S. Pan and J. Li, *Adv. Sci.*, 2022, **9**, 2106120.

26 X. Zhang, H. Wu, Z. Hu, J. Wang, Y. Wu and H. Yu, *Adv. Opt. Mater.*, 2024, **12**, 2301735.

27 J. Zhou, K. Hou, Y. Chu, Z. Yang, J. Li and S. Pan, *Small*, 2024, **20**, 2308806.

28 B.-W. Liu, X.-M. Jiang, H.-Y. Zeng and G.-C. Guo, *J. Am. Chem. Soc.*, 2020, **142**, 10641–10645.

29 B.-W. Liu, X.-M. Jiang, B.-X. Li, H.-Y. Zeng and G.-C. Guo, *Angew. Chem., Int. Ed.*, 2020, **59**, 4856–4859.

30 L. Wang, C. Tu, J. Zhou, Y. Chu, Z. Yang, S. Pan and J. Li, *Adv. Opt. Mater.*, 2023, **12**, 2301634.

31 J. Zhou, L. Wang, Y. Chu, H. Wang, S. Pan and J. Li, *Adv. Opt. Mater.*, 2023, **11**, 2300736.

32 B.-W. Liu, H.-Y. Zeng, X.-M. Jiang, G.-E. Wang, S.-F. Li, L. Xu and G.-C. Guo, *Chem. Sci.*, 2016, **7**, 6273–6277.

33 H. Chen, Y.-Y. Li, B. Li, P.-F. Liu, H. Lin, Q.-L. Zhu and X.-T. Wu, *Chem. Mater.*, 2020, **32**, 8012–8019.

34 B.-W. Liu, S.-M. Pei, X.-M. Jiang and G.-C. Guo, *Mater. Horiz.*, 2022, **9**, 1513–1517.

35 M. Yan, C.-L. Hu, R.-L. Tang, W.-D. Yao, W. Liu and S.-P. Guo, *Chem. Sci.*, 2024, **15**, 8500–8505.

36 J. Xu and K. Wu, *Coord. Chem. Rev.*, 2023, **486**, 215139.

37 X. Liu, Y.-C. Yang, M.-Y. Li, L. Chen and L.-M. Wu, *Chem. Soc. Rev.*, 2023, **52**, 8699–8720.

38 Z.-X. Wu, W.-F. Chen, X.-M. Jiang, B.-W. Liu and G.-C. Guo, *Chem. Mater.*, 2024, **36**, 3444–3451.

39 W.-F. Chen, B.-W. Liu, S.-M. Pei, X.-M. Jiang and G.-C. Guo, *Adv. Sci.*, 2023, **10**, 2207630.

40 J. Zhou, H. Wang, J. Liu, X. Su, Y. Chu, J. Qu and X. Jiang, *Inorg. Chem. Front.*, 2024, **11**, 2681–2689.

41 S. Toso, Q. A. Akkerman, B. Martín-García, M. Prato, J. Zito, I. Infante, Z. Dang, A. Moliterni, C. Giannini, E. Bladt, I. Lobato, J. Ramade, S. Bals, J. Buha, D. Spirito, E. Mugnaioli, M. Gemmi and L. Manna, *J. Am. Chem. Soc.*, 2020, **142**, 10198–10211.

42 J. Wang, H. Wu, H. Yu, Z. Hu, J. Wang and Y. Wu, *Adv. Opt. Mater.*, 2022, **10**, 2102673.

43 D. Ni, S. Guo, K. M. Powderly, R. Zhong and R. J. Cava, *J. Solid State Chem.*, 2019, **280**, 120982.

44 L. Bindi, A. Garavelli, D. Pinto, G. Pratesi and F. Vurro, *J. Solid State Chem.*, 2008, **181**, 306–312.

45 A. N. Roth, Y. Chen, A. Santhiran, J. Opare-Addo, E. Gi, E. A. Smith, A. J. Rossini and J. Vela, *Chem. Sci.*, 2023, **14**, 12331–12338.

46 M. Yan, R.-L. Tang, W. Zhou, W. Liu and S.-P. Guo, *Dalton Trans.*, 2022, **51**, 12921–12927.

47 L.-T. Jiang, M.-Z. Li, X.-M. Jiang, B.-W. Liu and G.-C. Guo, *Dalton Trans.*, 2022, **51**, 6638–6645.

48 R. Nie, B. Kim, S.-T. Hong and S. I. Seok, *ACS Energy Lett.*, 2018, **3**, 2376–2382.

49 H. Wang, G. Chen, J. Xu, Y. Xu and Q. Yang, *Cryst. Growth Des.*, 2018, **18**, 1987–1994.

50 Z. Lin, K. Feng, H. Tu, L. Kang, Z. Lin, J. Yao and Y. Wu, *J. Alloys Compd.*, 2014, **611**, 422–426.

51 J. Androulakis, S. C. Peter, H. Li, C. D. Malliakas, J. A. Peters, Z. Liu, B. W. Wessels, J.-H. Song, H. Jin, A. J. Freeman and M. G. Kanatzidis, *Adv. Mater.*, 2011, **23**, 4163–4167.

52 J.-X. Zhang, P. Feng, M.-Y. Ran, X.-T. Wu, H. Lin and Q.-L. Zhu, *Coord. Chem. Rev.*, 2024, **502**, 215617.

53 J. Chen, C. Lin, X. Jiang, G. Yang, M. Luo, X. Zhao, B. Li, G. Peng, N. Ye, Z. Hu, J. Wang and Y. Wu, *Mater. Horiz.*, 2023, **10**, 2876–2882.

54 Y. Guo, Y. Deng, T. Zheng, L. Huang, D. Gao, J. Bi and G. Zou, *Inorg. Chem. Front.*, 2022, **9**, 440–447.

55 J. Li, J. Shen, Z. Li, X. Li, Z. Sun, Z. Hu and S. Huang, *Mater. Lett.*, 2013, **92**, 330–333.

56 X. Wang, J. Li, Z. Zhao, S. Huang and W. Xie, *J. Appl. Phys.*, 2012, **112**, 023701.

57 F. van den Akker and W. G. J. Hol, *Acta Crystallogr., Sect. D: Biol. Crystallogr.*, 1999, **55**, 206–218.

58 G. M. Sheldrick, *Acta Crystallogr., Sect. A: Found. Crystallogr.*, 2008, **64**, 112–122.

59 A. L. Spek, *J. Appl. Crystallogr.*, 2003, **36**, 7–13.

60 S. K. Kurtz and T. T. Perry, *J. Appl. Phys.*, 1968, **39**, 3798–3813.

61 H. Qiu, F. Li, Z. Li, Z. Yang, S. Pan and M. Mutailipu, *J. Am. Chem. Soc.*, 2023, **145**, 24401–24407.

62 Y. Chu, H. Wang, Q. Chen, X. Su, Z. Chen, Z. Yang, J. Li and S. Pan, *Adv. Funct. Mater.*, 2024, **34**, 2314933.

63 Y. Chu, H. Wang, T. Abutukadi, Z. Li, M. Mutailipu, X. Su, Z. Yang, J. Li and S. Pan, *Small*, 2023, **19**, 2305074.

64 J. Zhou, Z. Fan, K. Zhang, Z. Yang, S. Pan and J. Li, *Mater. Horiz.*, 2023, **10**, 619–624.

65 L. Wang, D. Chu, D. Yin, C. Xie, Z. Yang, J. Li and S. Pan, *Mater. Today Phys.*, 2023, **38**, 101245.

66 C. Shen, F. Zhang, T. Sasaki, C. Eerdun, M. Hayashi, H.-W. Wang, K. Tominaga, M. Mutailipu and S. Pan, *Angew. Chem., Int. Ed.*, 2024, **63**, e202319121.

67 J. P. Perdew, K. Burke and M. Ernzerhof, *Phys. Rev. Lett.*, 1996, **77**, 3865–3868.

68 M. Gerwig, M. Schwarz, E. Brendler and E. Kroke, *Eur. J. Inorg. Chem.*, 2016, **2016**, 4557–4560.

69 A. B. Delpeuch, F. Maillard, M. Chatenet, P. Soudant and C. Cremers, *Appl. Catal., B*, 2016, **181**, 672–680.

70 L. Luo, L. Wang, J. Chen, J. Zhou, Z. Yang, S. Pan and J. Li, *J. Am. Chem. Soc.*, 2022, **144**, 21916–21925.

71 X. Zhang, H. Wu, Z. Hu, J. Wang, Y. Wu and H. Yu, *Adv. Opt. Mater.*, 2024, **12**, 2301735.

72 Y. Xu, C. Lin, D. Zhao, B. Li, L. Cao, N. Ye and M. Luo, *Scr. Mater.*, 2022, **208**, 114347.

73 M.-Y. Ran, S.-H. Zhou, W.-B. Wei, A.-Y. Wang, X.-T. Wu, H. Lin and Q.-L. Zhu, *Inorg. Chem. Front.*, 2024, **11**, 1890–1898.

74 A. Abudurusuli, J. Li and S. Pan, *Dalton Trans.*, 2021, **50**, 3155–3160.